Photoresponsive supramolecular soft materials in aqueous media

Chen, Shaoyu

DOI:
10.33612/diss.107818650

6

Chapter 6

Supramolecular Assembly Transformations of a Molecular Motor Amphiphile Controls Macroscopic Foam Properties

---

Manuscript:

Shaoyu Chen, Franco King-Chi Leung,* Marc C. A. Stuart, Chaoxia Wang* and Ben L. Feringa*

Abstract: Stimuli-responsive supramolecular assemblies controlling macroscopic transformations with high structural fluidity, *i.e.*, foam properties, have extensive potential applications in soft materials ranging from biomedical systems to industrial processes, *e.g.*, textile coloring processes. However, to identify the key processes for amplification from molecular motions to macroscopic level is of fundamentally importance for exerting the full potential of macroscopic structural transformation by external stimuli. In this chapter, we demonstrate an approach that allows control of the supramolecular assembly transformation in aqueous media and as a consequence its macroscopic foam properties, *e.g.,* foamability and foam stability, by large geometrical transformations of dual light/heat stimuli-responsive molecular motor amphiphiles. Detailed insight into the reversible photoisomerization and thermal helix inversion at the molecular level, supramolecular assembly transformations at the microscopic level, as well as the stimuli-responsive foam properties at the macroscopic level, as determined by absorption and NMR spectroscopies, electronic microscopy, foamability and *in-situ* surface tension measurements, are presented. By selective use of external stimuli, *e.g.,* light or heat, multiple states and properties of macroscopic foams can be controlled with a very dilute aqueous solution of the motor amphiphile (0.2 weight%), demonstrating the potential of multiple stimuli-responsive supramolecular systems based on an identical molecular structure and providing opportunities for future stimuli-responsive soft materials.

6.1 Introduction

Controlled supramolecular polymerization of biomolecules into functional assembled structures with low structural fluidity, *e.g.,* cytoskeleton filaments,[1,2] flagellar filaments of bacteria,[3,4] and high structural fluidity, *e.g.,* cell membrane,[5,6] serves key roles in correct functioning of biological processes. Inspired by natural supramolecular polymers,[1–4] the delicate structural tunability and stimuli-responsiveness of synthetic supramolecular polymers[7–16] in aqueous media allow sophisticated bioinspired functionality.[8–19] A molecular design with precise control of molecular organization and cooperativity allows energy conversion and amplification from nanometer to macroscopic length-scales and induces mechanical response[20–30] in hierarchical supramolecular assemblies.[31–38] Numerous amphiphilic molecular machines can assemble from one-dimensional (1D) supramolecular systems with low structural fluidity at microscopic length-scales to various three-dimension (3D) macroscopic supramolecular structures, to gain full control of macroscopic structural transformations by the manipulation of stimuli-responsive molecular motions. Using external stimuli, *e.g.,* pH,[38] heat,[39] and light,[40–45] the isomerization of the stimuli-responsive molecular machines can induce a macroscopic rupture of a 3D randomly entangled supramolecular structures from a gel-state into a solution-state. In addition to gel-sol transformation, we recently reported that a photoresponsive hierarchical supramolecular macroscopic string of a motor amphiphile allows the amplification of molecular rotation to macroscopic muscle-like contraction.[31–33] However, to sustain the macroscopic structural transformations usually requires a high concentration of stimuli-responsive units and high structurally ordered and rigid supramolecular assemblies.[31–33,38,39] Alternatively, as inspired by nature, *e.g.*, cell membrane, a supramolecular assembly with high structural fluidity can potentially be constructed with minimized amount of stimuli-responsive units that might allow a more effective energy conversion and amplification from nanometer length-scale motions to macroscopic structural transformations. By purging with air into an aqueous solution of an amphiphilic molecular structure (in general below 1.0 weight%), macroscopic foams with high structural fluidity are generated by dispersing air bubbles in the aqueous phase.[46–48] The foam structure spans over multi-length-scales from nanometer dimensions to macroscopic levels.[48] To provide precise control of macroscopic foam properties, *e.g.,* foamability and foam stability, one can take advantage of the isomerization of stimuli-responsive amphiphilic structures at molecular length-scales.[49–60]

Recently, we and others have demonstrated photoresponsive foams of azobenzene amphiphiles[51–60] for controlling foam rupture upon irradiation. However, to identify the key processes for energy conversion from nanometer length-scale motions to macroscopic structural transformations, *i.e.*, macroscopic foam rupture, remains

highly challenging, possibly due to an unavoidable fast reverse isomerization of the azobenzene chromophore. The fast switching back of azobenzene limits the controllability of the macroscopic foam properties. The development of a stimuli-responsive amphiphile with steady foam properties not only allows the identification of key processes for amplification but also precisely controls multiple states of foamability and foam stability. Molecular motors can be controlled with high precision by two orthogonal external stimuli, light and heat, to sustain a unidirectional rotation involving four distinct isomerization states. We envision that molecular motor amphiphiles hold significant prospects for the development of multiple states macroscopic foams with minimized amount of stimuli-responsive units and the potential identification of the key processes for amplification from nanometer length-scale motions to macroscopic foam properties. We previously reported that motor amphiphiles composed of a second generation molecular motor core doping into lipids provided supramolecular assembly transformations, but extra freeze-thaw cycles were required in the transformation processes.[61–63] Furthermore, the nanofibers of motor amphiphiles employed in artificial muscle-like motions showed no significant assembly transformations upon photoirradiation.[31–33] To sustain a large geometrical transformation, the change in packing parameters between *trans*- and *cis*-isomers,[64] is of fundamentally importance for generating assembly transformations from an identical molecular design upon photoisomerization. In this context, in the present design the molecular motor amphiphile contains a hydrophilic chain with a charged end-group and a hydrophobic alkyl chain connected to a first-generation molecular motor core (Figure 6.1).

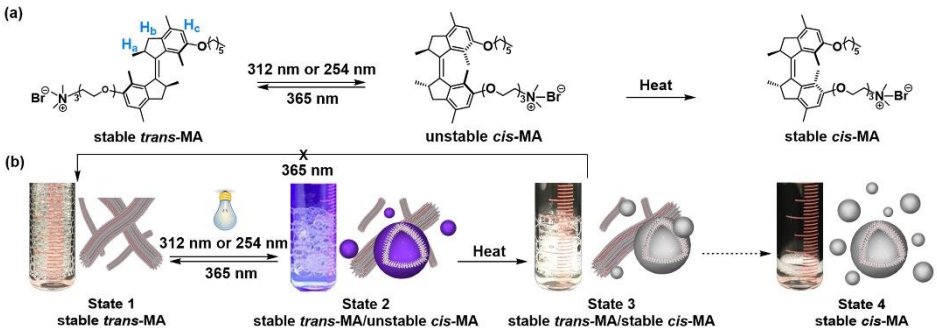

Figure 6.1 *Schematic illustrations of (a) the reversible photoisomerization and thermal helix inversion of molecular motor amphiphile (**MA**) and (b) the controlled macroscopic foaming processes due to structural transformations in the supramolecular assembly.*

If the motor unit adopts a *trans* geometry, the two side chains will be remote from each other and we expect a lower packing parameter in the structure (*e.g.,* worm-like

micelle), while the *cis* form will bring the two side chains in close proximity, allowing for a higher packing parameter (*e.g.,* vesicle). Large geometrical transformations of motor amphiphiles might enable supramolecular assembly transformations, without co-assembly with other lipids, for controlling macroscopic foam properties. By elucidating the key assembly transformation processes, this could open up new prospects towards the development of controllable stimuli-responsive materials.

6.2 Results and Discussion

6.2.1 Molecular design and synthesis

The motor amphiphile (**MA**) was designed with a first-generation molecular motor core, attached with an alkyl chain to form the hydrophobic part and a quaternary ammonium moiety connected via a triethylene glycol-linker to form the hydrophilic part. The synthesis is summarized in Scheme 6.1. Phenolic motor **1** and 1,2-bis(2-bromoethoxy)-ethane (**3**) were prepared according to reported procedures[65,66] and the stable *trans*-**1** and stable *cis*-**1** were isolated by flash column chromatography.[65] Motor **2** was obtained by a Williamson ether formation in the presence of 1-bromohexane, tetrabutylammonium iodide, and K_2CO_3 in acetonitrile. The freshly prepared motor **2** was treated with 1,2-bis(2-bromoethoxy)-ethane (**3**) and Cs_2CO_3 in DMF to afford *trans*-**4** and *cis*-**4** in 43% and 50% yields, respectively. Subsequent reaction of motor **4** with trimethylamine gave the corresponding stable *trans*-**MA** and stable *cis*-**MA** in 90% yield. The detailed procedures of synthesis and characterization of new molecules are provided in the section of Experimental Data.

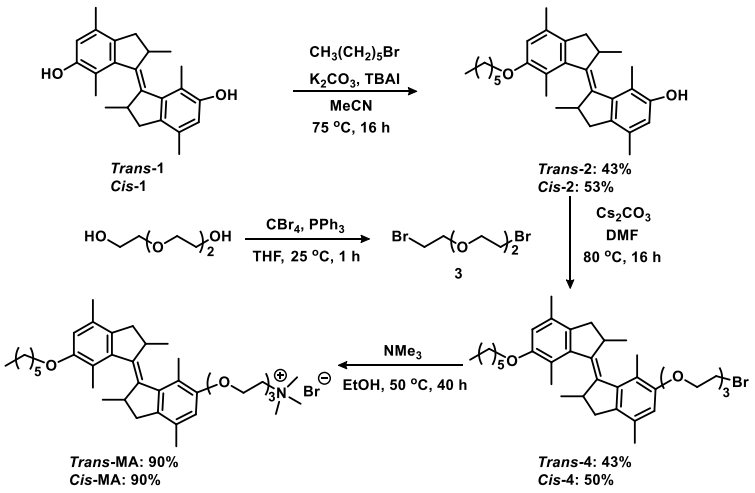

Scheme 6.1 *Synthesis of stable trans-**MA** and stable cis-**MA**.*

6.2.2 Photoisomerization and thermal helix inversion steps to control packing parameters of MA

For the first-generation motor core of **MA**, its 360° unidirectional rotary cycle involves four stages, in which one half of the molecule rotates with respect to the other half around a central double bond via two photochemical isomerizations and two thermal helix inversion (THI) steps. Because of the fast thermal isomerization between unstable *trans*-**MA** and stable *trans*-**MA**,[67,68] the reversible photoisomerization from stable *trans*-**MA** to unstable *cis*-**MA** as well as the THI between unstable *cis*-**MA** and stable *cis*-**MA** are employed for the control of the molecular geometrical transformations, *i.e.,* packing parameter transformations (Figure 6.1). A methanol solution of stable *trans*-**MA** (30 μM) shows a strong absorption band at 260–340 nm in the UV-vis absorption spectrum (Figure 6.2a). A new absorption band appears at 350–385 nm with a clear isosbestic point at 330 nm upon irradiating with 312 nm light for 6 min at 5 °C (Figure 6.2a), indicating a selective photoisomerization process from stable *trans*-**MA** to unstable *cis*-**MA**. The resulting solution, prepared by photoisomerization from stable *trans*-**MA** to unstable *cis*-**MA**, was able to switch back to stable *trans*-**MA** upon 365 nm light irradiation for 1 min (Figure 6.2b), or to rotate selectively from unstable *cis*-**MA** to stable *cis*-**MA** by heating at 55 °C for 2 h via the THI step (Figure 6.2c). A CD_3OD solution of stable *trans*-**MA** (2.0 mM), irradiated with 312 nm light for 6 min, shows distinctive proton shifts in ^1H NMR spectra upon photoisomerization (Figure 6.3a-b). The hydrogen atoms of the methyl groups adjacent to the stereogenic centers (H_a), aliphatic protons (H_b) and aromatic protons (H_c) are highlighted for clarity (Figure 6.1, Figure 6.3). The proton signals of H_a δ = 1.10 ppm and H_b δ = 2.18 ppm shift downfield to H_a δ = 1.23 ppm and H_b δ = 2.60 ppm, respectively, while a upfield shift of H_c is observed with an unstable *cis*-**MA**/stable *trans*-**MA** isomers ratio of 1 : 1, upon 312 nm light irradiation for 6 min (Figure 6.3a-b). Notably, the obtained unstable *cis*-**MA** in the solution can be fully switched back to stable *trans*-**MA** with 365 nm light irradiation, or selectively isomerized to stable *cis*-**MA** by heating at 55 °C for 2 h via the THI step with a distinct set of proton shifts (H_a δ = 1.23 to δ = 1.05; H_b δ = 2.60 ppm to δ = 2.41) (Figure 6.3b–c). By Eyring analysis, activation parameters of the unstable *cis*-**MA** to stable *cis*-**MA** conversion were obtained with the standard Gibbs energy of activation ($\Delta^{\ddagger}G°$ = 100.0 kJ mol^{-1}) and a half-life of 10.6 h at 25 °C (Figure 6.4, Table 6.1). The results clearly demonstrated that the molecular geometrical transformations could be controlled selectively by orthogonal external stimuli light and heat.

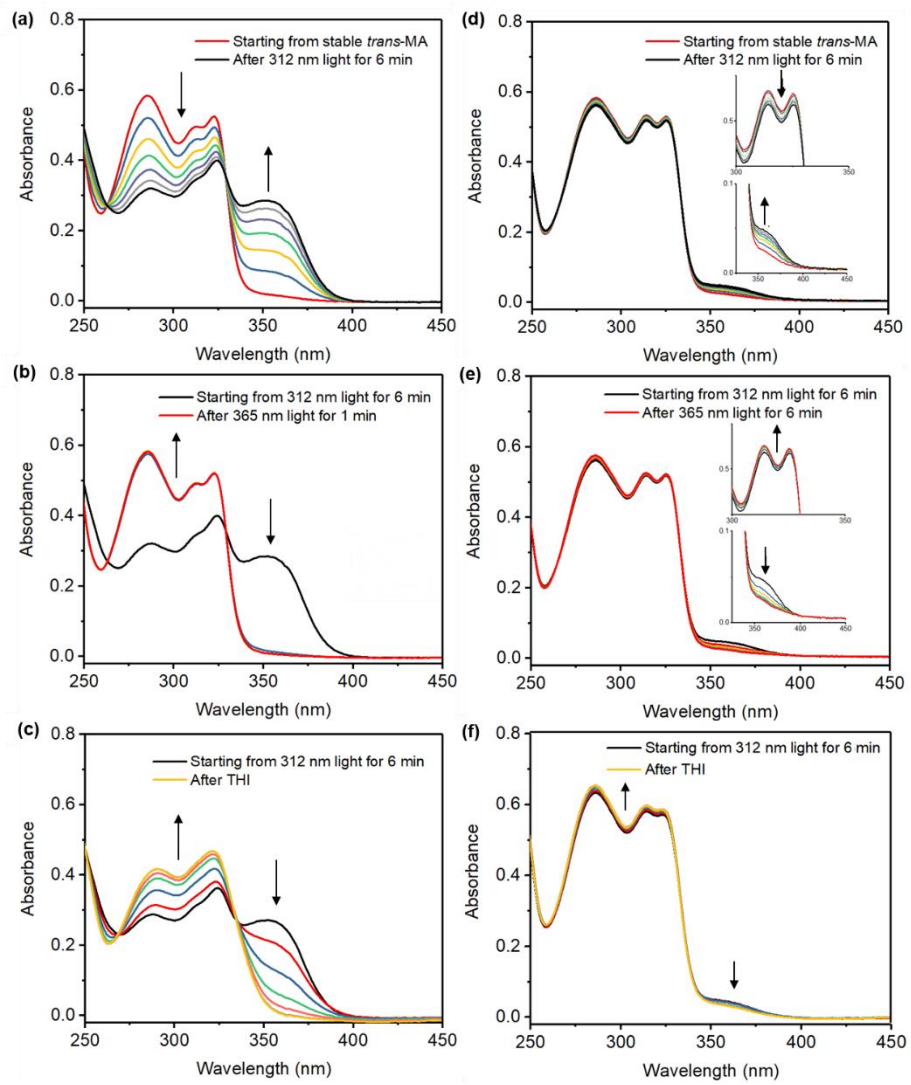

Figure 6.2 *UV-vis absorption spectra of the 180° rotation process of* ***MA*** *(30 μM), from stable trans-****MA*** *to stable cis-****MA*** *in MeOH and buffer (Tris-EDTA, pH 7.4). (a) A freshly prepared MeOH solution of stable trans-****MA*** *was irradiated with 312 nm light, (b) followed by exposure to 365 nm light or (c) heating at 55 °C for 2 h. (d) A freshly prepared buffer solution of stable trans-****MA*** *was irradiated with 312 nm light, (e) followed by exposure to 365 nm light or (f) heating at 55 °C for 2 h. All the photoirradiations were performed at 5 °C for 6 min.*

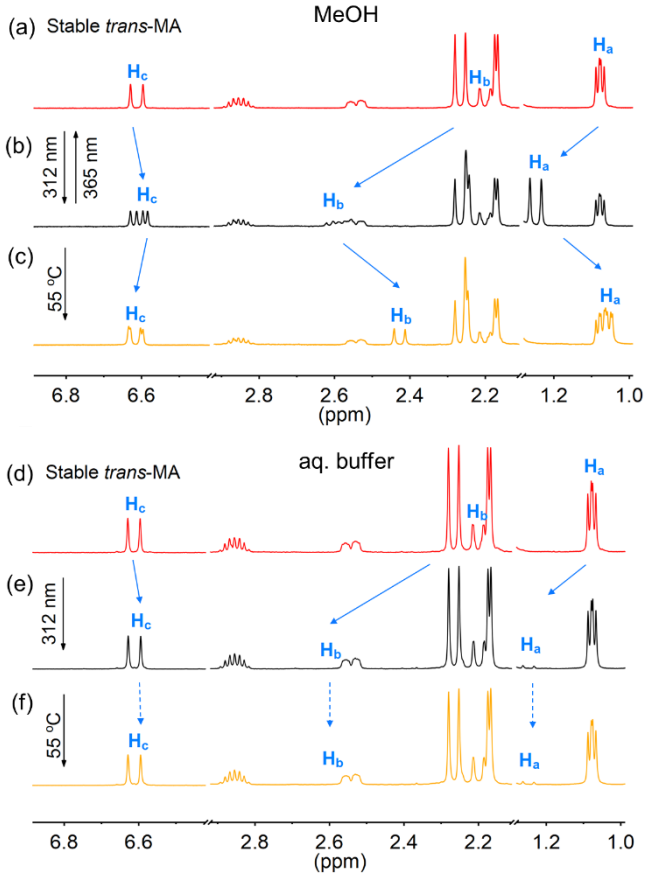

Figure 6.3 *Selected region of ^{1}H NMR spectra of **MA** (2.0 mM, CD_3OD, 25 °C, 500 MHz). (a) A CD_3OD solution of stable trans-**MA** was (b) irradiated with 312 nm light, (c) followed by heating at 55 °C for 2 h. (d) A Tris-EDTA buffer solution (pH 7.4) of stable trans-**MA** was (e) irradiated with 312 nm light, (c) followed by heating at 55 °C for 2 h. The buffer solutions after light irradiation or THI step were subjected to a freeze-drying process and then dissolved in CD_3OD for ^{1}H NMR measurement. All the photoirradiations were performed at 5 °C for 6 min. For the proton assignment, see Figure 6.1.*

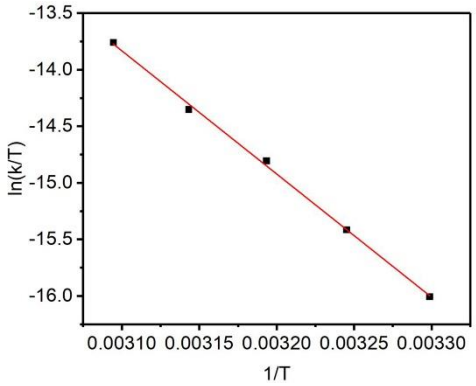

Figure 6.4 *Kinetic studies of the thermal helix inversion step of* ***MA*** *from unstable cis-****MA*** *to stable cis-****MA*** *by UV-vis absorption spectral changes at 365 nm at five different temperature conditions in MeOH (30 °C, 35 °C, 40 °C, 45 °C and 50 °C).*

Table 6.1 *Activation parameters and half-lives of* ***MA*** *from unstable cis-****MA*** *to stable cis-****MA****.*

Solvent	$t_{1/2}$ at 298.18 K (h)	$\Delta^{\ddagger}G°$ (kJ/mol)	$\Delta^{\ddagger}H°$ (kJ/mol)	$\Delta^{\ddagger}S°$ (J/K/mol)
MeOH	~10.6	100.0±2.8	90.6±2.0	–31.7±6.5

A Tris-EDTA buffer (pH 7.4) solution of stable *trans*-**MA** (30 μM) shows an absorption band at 260–340 nm in the absorption spectrum (Figure 6.2d), however, only a weak absorption band is observed at 350–385 nm upon irradiating with 312 nm light for 6 min at 5 °C (Figure 6.2d). Consequently, only an unstable *cis*-**MA**/stable *trans*-**MA** isomer ratio of 1 : 22 is obtained upon 312 nm light irradiation for 6 min of a buffer solution of stable *trans*-**MA** (2.0 mM) in ^{1}H NMR analysis (Figure 6.3d–e). As expected, only limited ratiometric changes in absorption spectra and proton signal shifts in ^{1}H NMR studies are observed with a heating process (55 °C, 2 h) of the stable *trans*-**MA** buffer solution obtained after 312 nm irradiation for 6 min (Figures 6.2d–f and 6.3d–f). To allow a more efficient photoisomerization in aqueous media, a light source with higher light intensity was employed (λ_{max} = 254 nm). A higher unstable *cis*-**MA**/stable *trans*-**MA** isomers ratio of 1 : 13 was confirmed upon 254 nm light irradiation for 6 min of a stable *trans*-**MA** buffer solution (2.0 mM) at 5°C by ^{1}H NMR. As expected, a higher unstable *cis*-**MA**/stable *trans*-**MA** isomers ratio of 1 : 6 is observed upon 254 nm light irradiation at 25 °C (Figure 6.5a-b. It should be noted that the ratio of 1 : 6 was obtained upon irradiation for only 6 min, not reaching the photostationary state, but this was sufficient to induce significant self-assembly transformations and macroscopic foams ruptures, as shown in the sections of 6.2.3 and 6.2.4. Prolonging the light irradiation, decomposition of **MA** was observed. For the detailed investigation of decomposition,

see section B in the Appendix). Furthermore, similar to isomerization in methanol, the obtained unstable *cis*-**MA** in buffer solution, prepared by the photoisomerization of the stable *trans*-**MA** solution with 254 nm light irradiation at 25 °C for 6 min, is able to switch back to stable *trans*-**MA** by 365 nm light irradiation, or to rotate selectively to stable *cis*-**MA** by heating at 55 °C for 24 h via the THI step (Figure 6.5). The results indicated the molecular geometrical transformation could be controlled selectively by orthogonal external stimuli not only in organic solvents but also in aqueous media, allowing for further investigations of molecular geometrical transformations at higher assembling length-scales in aqueous media.

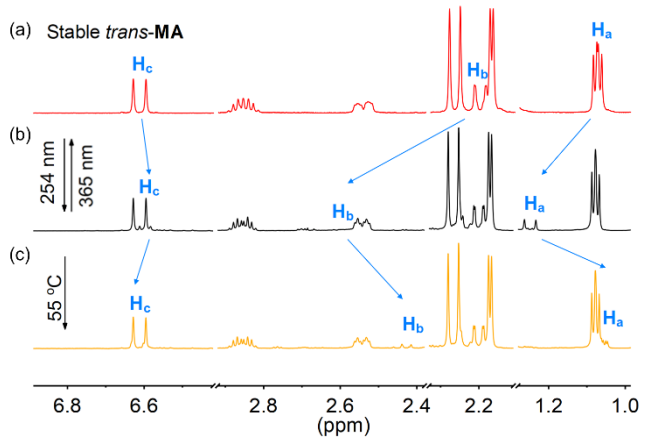

Figure 6.5 *Aromatic and aliphatic region in the ^{1}H NMR spectra during the isomerization process of* ***MA*** *(2.0 mM, CD_3OD, 25 °C, 500 MHz). (a) A buffer solution of stable trans-****MA*** *was (b) irradiated with 254 nm light at 25 °C for 6 min, (c) followed by heating at 55 °C for 24 h. The buffer solutions after light irradiation or THI step were subjected for a freeze-drying process and then dissolved in CD_3OD for ^{1}H NMR studies. For the proton assignment, see Figure 6.1.*

6.2.3 Supramolecular assembly transformation at microscopic length-scales

Freshly prepared Tris-EDTA buffer solutions (pH 7.4) of stable *trans*-**MA** (2.0 mM) were diluted into a range of concentrations from 2.0 x 10^{-5} to 2.0 mM for the determination of the critical aggregation concentration (CAC) by using a Nile Red fluorescence assay (NRFA), which probes the internal hydrophobicity of assemblies.[32,69] A significant decrease in blue shift is observed when the concentration of the stable *trans*-**MA** buffer solution is diluted below 0.1 mM (Figure 6.6a). The CAC of the stable *trans*-**MA** buffer solution was determined as 5 μM. It is noted that the concentration in the buffer solutions of stable *trans*-**MA** used in the UV-vis absorption (30 μM) and ^{1}H NMR spectroscopic studies (2.0 mM) were

higher than its CAC. The freshly prepared buffer solution of stable *trans*-**MA** (2.0 mM) was irradiated with 254 nm light for 6 min at 25 °C, whereupon the CAC of the resulting solution of **MA** increased to 12 μM (Figure 6.6b). The results imply a possible supramolecular assembly transformation occurred upon photoirradiation in the buffer solution of **MA**.

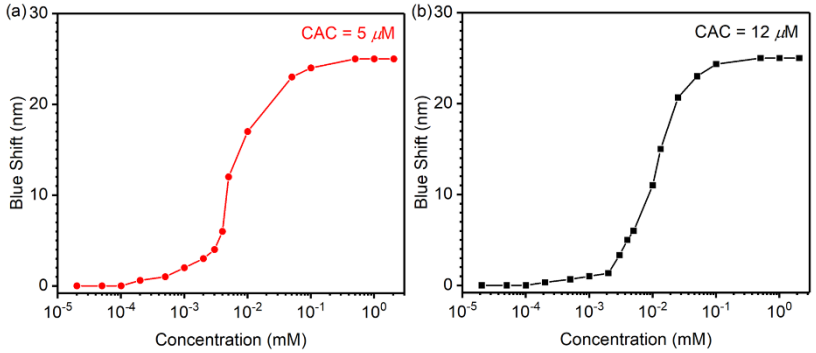

Figure 6.6 *Nile Red fluorescence assay for the determination of the critical aggregation concentration of buffer solutions of stable trans-**MA** (concentration: 2.0 x 10^{-5} to 2.0 mM) (a) before and (b) after irradiation with 254 nm light for 6 min at 25 °C.*

The supramolecular assemblies of **MA** were imaged using cryogenic transmission electron microscopy (cryo-TEM) to investigate their solution-state morphologies. Worm-like micelle structures with hundreds of nanometers to micrometers in length are observed by cryo-TEM from the buffer solution of stable *trans*-**MA** (concentration: 2.0 mM, Figure 6.7a). A mixture of worm-like micelles (length: ~200 nm to ~1 μm) and vesicles (diameter: 50~200 nm) is observed in the cryo-TEM image of the same solution after irradiated with 254 nm for 6 min at 25 °C (Figure 6.7b). The identical sample was employed in the ^{1}H NMR study (Figure 6.5b), indicating that the presence of only ~15% of unstable *cis*-**MA** in the mixture with stable *trans*-**MA** was able to induce drastic supramolecular assembly transformations of **MA** in aqueous media.

Notably, the supramolecular assemblies of the mixture of worm-like micelles and vesicles remain stable for 4 h at 25 °C in the dark conditions (Figure 6.7d–f), but can be reversibly converted back to worm-like micelles after exposing to 365 nm light for 6 min (Figure 6.7c). The identical sample was used in the ^{1}H NMR study. The conversion of the supramolecular assemblies from the mixture of worm-like micelles and vesicles back to worm-like micelles was possibly attributed to the reversible geometrical transformation from unstable *cis*-**MA** to stable *trans*-**MA**, upon 365 nm light irradiation for 6 min at 25 °C. The buffer solution of **MA** irradiated with 254 nm light for 6 min and subsequently heated at 55 °C for 24 h shows a mixture of

worm-like micelles and vesicles (Figure 6.7g). Although the obtained morphologies are essentially identical to that of observed in the sample of stable *trans*-**MA** irradiated with 254 nm for 6 min at 25 °C (Figure 6.7b), the obtained vesicle assemblies remained stable after further photoirradiation with 365 nm light (Figure 6.7h). Moreover, a freshly prepared buffer solution of stable *cis*-**MA** (2.0 mM) showed vesicle assemblies with diameters from 50 nm to ~200 nm (Figure 6.7i) similar to that of sample of stable *trans*-**MA** irradiated with 254 nm light and subsequently heated at 55 °C for 24 h (Figure 6.7g), suggesting that the obtained mixture of worm-like micelle and vesicle structures (Figure 6.7g) are possibly composed of stable *trans*-**MA**/stable *cis*-**MA**.

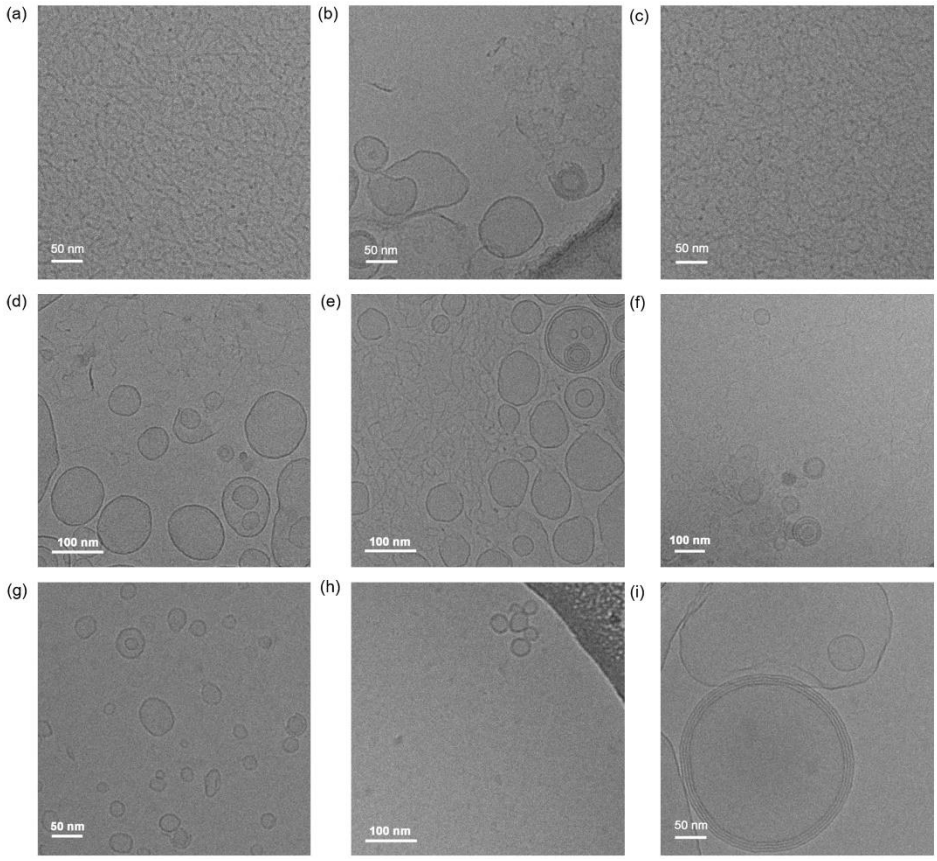

Figure 6.7 *Cryo-TEM images of Tris-EDTA buffer solutions (pH 7.4) of* ***MA*** *(2.0 mM). (a) The buffer solution of trans-****MA*** *was (b) irradiated with 254 nm light, (c) followed by exposure to 365 nm light. The buffer solution of trans-****MA*** *irradiated with 254 nm light was kept in the dark at 25 °C for (d) 25 min, (e) 50 min and (f) 4 h. (g) The buffer solution of trans-****MA*** *irradiated with 254 nm light was gently heated at 55 °C for 24 h, (h) followed by 365 nm light irradiation. (i) A stable cis-****MA*** *solution (2.0 mM). All the photoirradiations were performed at 25 °C for 6 min.*

The results showed clearly that the manipulation of molecular geometrical transformations with external stimuli can provide the control of supramolecular assemblies from nanometers to hundreds of nanometers length-scales systematically. Namely, four states of supramolecular assemblies can be controlled (1) worm-like micelles from stable *trans*-**MA** only, (2) a mixture of worm-like micelles and vesicles from ~15% of unstable *cis*-**MA** in stable *trans*-**MA**, (3) a mixture of worm-like micelles and vesicles from a mixture of stable *cis*-**MA** in stable *trans*-**MA** which cannot be switched back by 365 nm irradiation, (4) vesicles from stable *cis*-**MA** only.

6.2.4 Macroscopic photoresponsive foam

Amphiphilic molecules can assemble into supramolecular aggregates in solutions and monolayers at air-water interfaces.[46–48] It is noted that both the supramolecular aggregates and monolayers are highly dependent on the concentration and molecular structure. Motor amphiphiles in aqueous media and at air-water interfaces might allow for controlling macroscopic phenomena by amplification of packing/organization due to geometrical changes. Stable foams were generated from a buffer solution of stable *trans*-**MA** (1.5 mM, 0.4 mL) by bubbling with a flow of argon gas (6 cm^3 min^{-1}) for 8 min in a quartz tube (Figure 6.8a). The buffer solution of stable *trans*-**MA** showed good foamability with a foaming ratio of ~8.3. However, no stable foam was formed by the identical preparation method from a buffer solution of stable *cis*-**MA** (Figure 6.8a). The foaming ratio (R) was calculated from the equation $R=V_{foam}/V_{liquid}$, in which V_{foam} and V_{liquid} referred to the foam volume and the original liquid volume to prepare foams, respectively.[60,70] A higher foaming ratio indicates a higher foamability. Drainage is one of the main processes resulting the destabilization of foams, which can be affected by the self-assembled structures in the bulk solutions. Given that long fibrillar assemblies can slow down the drainage process and no significant reduction of drainage process was observed with vesicle assemblies,[71–73] the worm-like micelle structures in the solution of stable *trans*-**MA** can proved a stable macroscopic foam structure. In sharp contrast, no stable foams were observed in the solution of stable *cis*-**MA**. These promising results provided a hint for the control of macroscopic foam formation and the related foam parameters by using the four states of supramolecular assemblies of **MA** (*vide infra*).

For a buffer solution of stable *trans*-**MA** (2.0 mM) by bubbling with a flow of argon gas (10 cm^3 min^{-1}) for 8 min (Figure 6.8b,c, sample 1), a higher foaming ratio (13.5 ± 0.3) is observed than that of the stable *trans*-**MA** buffer solution (1.5 mM, Figure 6.8a). It is noted that a very diluted stable *trans*-**MA** buffer solution (2.0 mM, containing 99.8 wt.% of buffer and 0.2 wt.% of **MA**) shows excellent foamability with a high foaming ratio and foams remain stable over 20 min at 25 °C without any sign of foam rupture (Figure 6.8b). Notably, a fast response of foam rupture, *i.e.*,

~57% of foams rupture, is observed after 254 nm light irradiation at 25 °C for 6 min (Figures 6.8b, sample 2). The obtained solutions after foam rupture were subjected for a freeze-drying process and studied by ^{1}H NMR (Figure 6.9a,b). An unstable *cis*-**MA**/stable *trans*-**MA** isomers ratio of 1 : 6 was observed, which is essentially identical to that of observed in the buffer solution of stable *trans*-**MA** irradiated with 254 nm light for 6 min at 25 °C (Figure 6.5a,b). The foam rupture is attributed to the supramolecular assembly transformations from worm-like micelles into the mixture of worm-like micelles and vesicles as imaged by cryo-TEM (Figure 6.7a,b). The solution obtained from foams rupture was bubbled with a flow of argon gas (10 cm^3 min^{-1}) for 8 min, which showed a lower foaming ratio of 8.6 ± 0.3 (Figure 6.8c, sample 2). Furthermore, the resulting solution of stable *trans*-**MA** irradiated with 254 nm light was subsequently exposed to 365 nm light for 6 min at 25 °C, generating stable foams again with a foaming ratio of 13.7 ± 0.3 (Figure 6.8c, sample 3) that was comparable to that of observed in the foam solution of stable *trans*-**MA** (2.0 mM, Figure 6.8b,c, sample 1). Additionally, the obtained solution shows a clear switching process from unstable *cis*-**MA** to stable *trans*-**MA** based on ^{1}H NMR spectra (Figure 6.9b,c). The restoration of foamability after sequential irradiation with 254 nm and then 365 nm light was attributed to the assembly transformations from state (2) the mixture of worm-like micelles and vesicles into state (1) worm-like micelles, as seen in cryo-TEM images (Figure 6.5b,c). Furthermore, the foams obtained from a solution of stable *trans*-**MA** after irradiation with 254 nm light and a subsequent heating at 55 °C for 24 h showed a foaming ratio of 8.9 ± 0.2 (Figure 6.8c, sample 4), which was comparable to that of observed in the foams obtained from the solution of stable *trans*-**MA** after irradiation with 254 nm light (8.6 ± 0.3, Figure 6.8c, sample 2). However, after the 254 nm light irradiated solutions of stable *trans*-**MA** being subjected to a THI process (55 ºC for 24 h), the foaming ratio of the resulting solution cannot switch back to the value of ~13 by exposure to 365 nm light (Figure 6.8c, sample 5). The results showed clearly that by manipulation of molecular geometrical transformations with light and heat stimuli, the macroscopic foaming ratio also can be finely controlled at four states, *i.e.*, (1) foaming ratio of ~13 from stable *trans*-**MA** only, (2) a reversible switching of foaming ratio between ~8 and ~13 from the photoisomerization of unstable *cis*-**MA** and stable *trans*-**MA**, (3) foaming ratio of ~8 from a mixture of stable *cis*-**MA** in stable *trans*-**MA** which cannot be switched back by 365 nm light irradiation, (4) no foams generation from stable *cis*-**MA** only (Figure 6.8c). The four states of foaming ratio manipulation are consistent with the four states of supramolecular assembly transformations (Figure 6.7), indicating the control of macroscopic foam properties by fine adjustment of supramolecular assemblies with orthogonal external stimuli, light (254 nm and 365 nm) and heat.

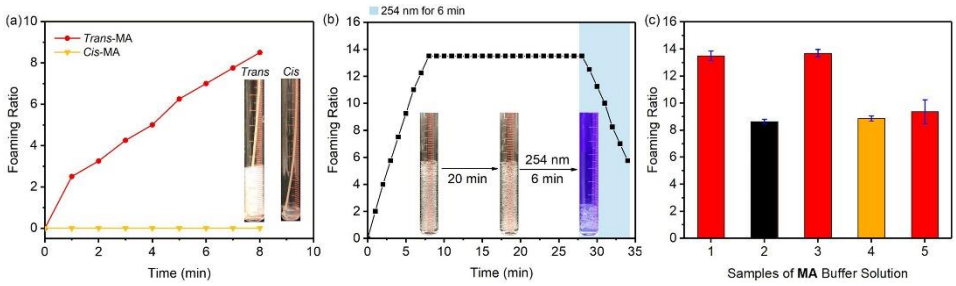

Figure 6.8 *(a) Foamability of stable trans-**MA** and stable cis-**MA** buffer solutions (1.5 mM, bubbling with a flow of argon gas, 6 cm^3 min^{-1} for 8 min). (b) Foams, prepared from a solution of stable trans-**MA** (2.0 mM) by bubbling with a flow of argon gas (10 cm^3 min^{-1} for 8 min), were kept at 25 °C for 20 min and then irradiated with 254 nm light for 6 min. (c) Foamability of stable trans-**MA** buffer solutions before and after photoirradiation and THI steps (2.0 mM, bubbling with a flow of argon gas, 10 cm^3 min^{-1} for 8 min). Stable trans-**MA** buffer solutions (sample 1) were irradiated with 254 nm light at 25 °C for 6 min (sample 2). The resulting solutions were exposed to 365 nm light at 25 °C for 6 min (sample 3) or heated at 55 °C for 24 h (sample 4). Sample 4 was subsequently irradiated with 365 nm light at 25 °C for 6 min to obtain sample 5.*

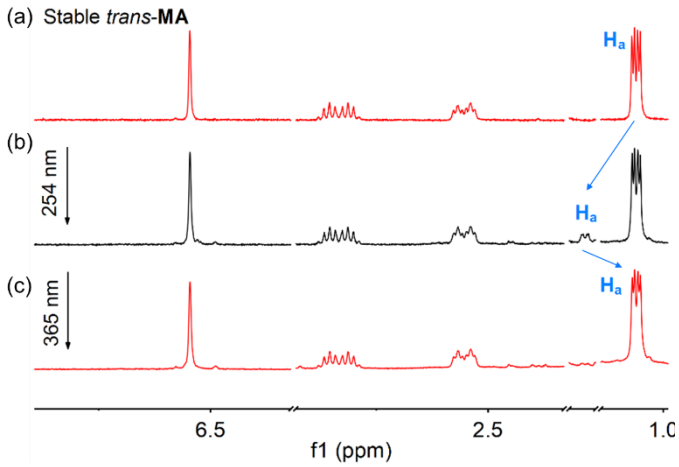

Figure 6.9 *Selected region of ^1H NMR spectra (500 MHz, 25 °C) of foams in sequential irradiation with 254 nm and 365 nm light for 6 min. (a) Buffer solutions of stable trans-**MA** (2.0 mM) were employed for foam preparation, (b) followed by irradiation with 254 nm light, (c) and then exposure to 365 nm light. The resulting solutions were subjected for a freeze-drying process and then dissolved in CD_2Cl_2 for ^1H NMR measurements. All the photoirradiations were performed at 25 °C for 6 min. After irradiating with 254 nm light, ~15% of unstable cis-**MA** was obtained. For the proton assignment, see Figure 6.1.*

Buffer solutions of stable *trans*-**MA** at 3.0 mM or 4.0 mM by bubbling with a flow of argon gas (10 cm^3 min^{-1} for 8 min) showed a comparable foaming ratio (Figure 6.10a,b) to the foams prepared from the stable *trans*-**MA** solution at 2.0 mM concentration (Figure 6.8b). The obtained foams, prepared from the stable *trans*-**MA** solutions (at 3.0 mM or 4.0 mM concentration), remained stable over 20 min at 25 °C, and upon exposure to 254 nm light for 6 min, 31% or 14% of foam ruptures are observed, respectively (Figure 6.10a,b). Moreover, the foaming properties can be reversibly tuned by alternating 254 nm light and 365 nm light irradiation over 10 cycles (Figure 6.10c).

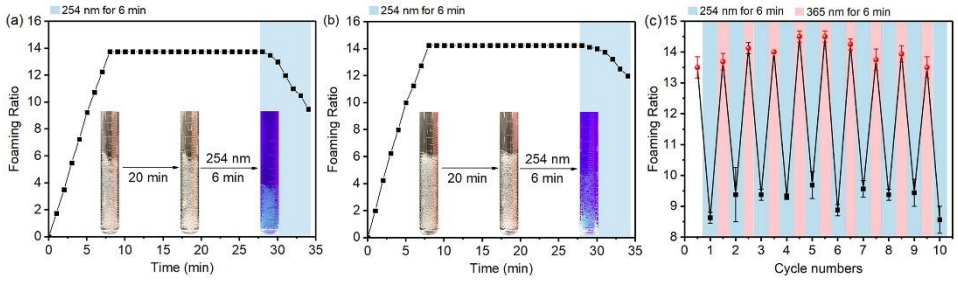

Figure 6.10 *Foams, prepared from solutions of stable trans-**MA** at (a) 3.0 mM and (b) 4.0 mM concentration by bubbling with a flow of argon gas (10 cm^3 min^{-1} for 8 min), were kept at 25 °C for 20 min, and then irradiated with 254 nm light for 6 min. (c) The change of foaming ratio of a **MA** buffer solution (2.0 mM) after 10 irradiation cycles by alternating 254 nm and 365 nm light.*

To provide insight into the molecular packing of **MA** at the air-water interface, an *in-situ* surface tension measurement was employed. The surface tension was determined by a drop-shape analysis system, which was based on the fitting of the pendant drop shape of the measured solutions with the Yong-Laplace equation of capillarity.[74–76] The detailed experimental setup and measurement conditions are provided in the section of Experimental Data. The surface tension of the stable *trans*-**MA** buffer solution (2 mM) remains stable at 33.1 mN/m (Figure 6.11a). A quick increase of surface tension from 33.1 mN/m to 33.9 mN/m was observed after irradiating the droplet of stable *trans*-**MA** with 254 nm light for 30 s. Furthermore, prolonging 254 nm light irradiation, the surface tension increased continuously to 35.3 mN/m until the droplet of stable *trans*-**MA** fell down at 5 min, thus the measurement was halted (Figure 6.11a). However, the surface tension of a Tris-EDTA buffer solution irradiated under the identical conditions almost remained stable at ~69.5 mN/m over 5 min (Figure 6.11b). A droplet of the stable *trans*-**MA** buffer solution (2 mM) without 254 nm light irradiation also shows a limited variation (only 0.5 mN/m increase) in 5 min (Figure 6.11c). The results clearly indicated that the significant increase of surface tension of the stable *trans*-**MA**

buffer solution (up to 2.43 mN/m) upon irradiation with 254 nm light was attributed to the photoisomerization of stable *trans*-**MA**.

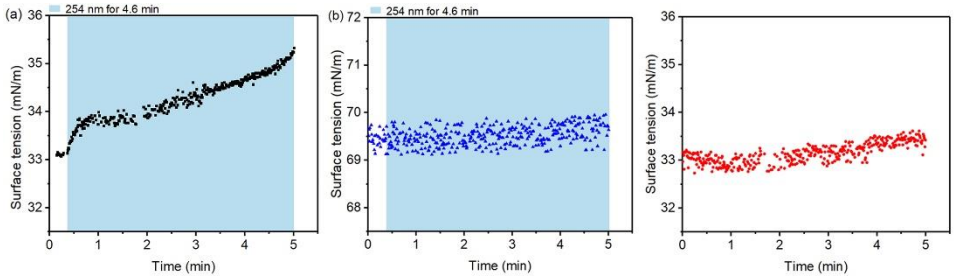

Figure 6.11 *In-situ surface tension measurement. (a) A buffer solution of stable trans-**MA** (2.0 mM) upon irradiating with 254 nm light over 4.6 min, until the droplet of stable trans-**MA** fell down at 5 min. (b) A buffer solution upon irradiating with 254 nm light for 4.6 min. (c) A buffer solution of stable trans-**MA** (2.0 mM) without 254 nm light irradiation.*

Following the photochemical isomerization of stable *trans*-**MA** to unstable *cis*-**MA**, a large geometrical transformation was observed, which in turn leads to a disturbance of molecular packing at air-water interfaces.[57] Based on the results of *in-situ* surface tension measurements, indeed, a gradual increase of surface tension (up to 2.43 mN/m) was observed, which was attributed to the desorption of unstable *cis*-**MA** from the air-water interfaces to the bulk solution, suggesting that a similar desorption of unstable *cis*-**MA** from the air-water interfaces to the foam films and plateau borders might occur (Figure 6.12).[74–76] On the basis of supramolecular assembly transformation at the microscopic length-scale, long fibrillar structures obtained from the solution of stable *trans*-**MA** resulted in the reduction of liquid drainage in foams, while a mixture of worm-like micelles and vesicles obtained from the solution of unstable *cis*-**MA**/stable *trans*-**MA** increased the destabilization of foams.[71–73] Furthermore, the corresponding transformation from worm-like micelles to the mixture of worm-like micelles and vesicles comes with an increase of CAC (Figure 6.6), which possibly facilitates the desorption of unstable *cis*-**MA** from the air-water interface to the foam films and plateau borders. In combination of the aforementioned variation of macroscopic foam parameters, as the ultimate result, foam rupture is observed.

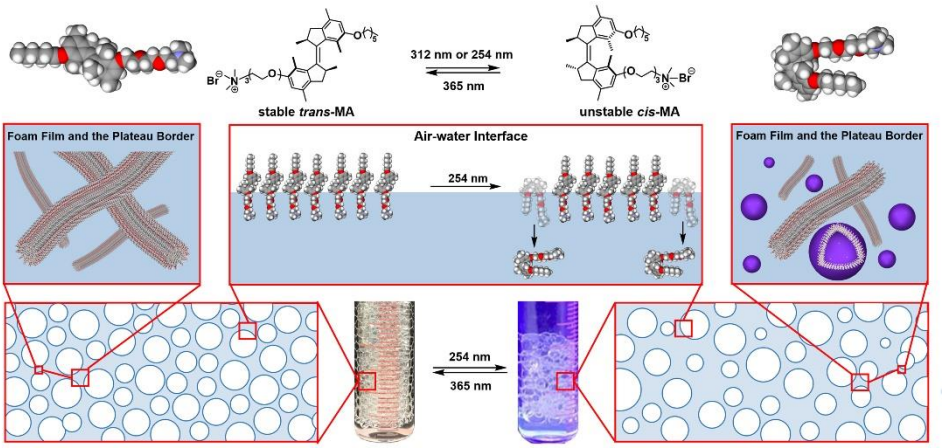

Figure 6.12 *Schematic illustration of supramolecular assembly transformations from stable trans-**MA** to unstable cis-**MA** upon 254 nm irradiation at air-water interfaces and in plateau borders.*

6.3 Conclusions

Motor amphiphile isomers were synthesized and the reversible photoisomerization and thermal helix inversion were followed by UV-vis absorption and proton NMR spectroscopies. As shown by NRFA, a clear increase of CAC of stable *trans*-**MA** was observed after photoirradiation. By sequential orthogonal control with light and heat, worm-like micelles of stable *trans*-**MA**, vesicles of stable *cis*-**MA**, and a mixture of worm-like micelles/vesicles of stable *trans*-**MA**/unstable *cis*-**MA** or stable *trans*-**MA**/stable *cis*-**MA** were obtained and analyzed by cryo-TEM. This method provided a systematic control of macroscopic foam properties to achieve a fine adjustment of foaming ratio over 10 cycles with a low content of **MA** in aqueous media (0.2 wt.%). The current approach demonstrates the dual control of multiple states macroscopic foam properties by supramolecular assembly transformations based on light/heat responsive motor amphiphiles. We also identified the key processes and parameters of amplification from molecular motions to macroscopic structural transformations. It might open up new prospects towards developments of controllable stimuli-responsive materials.

6.4 Acknowledgements

This work was supported financially by the China Scholarship Council (no. 201706790063 to S.Y.C.), the Croucher Foundation (Croucher Postdoctoral Fellowship to F.K.C.L.), the Netherlands Organization for Scientific Research (NWO-CW), the European Research Council (ERC; advanced grant no. 694345 to

B.L.F.), the Ministry of Education, Culture and Science (Gravitation program no. 024.001.035) and National Natural Science Foundation of China (21174055), National First-Class Discipline Program of Light Industry Technology and Engineering (LITE2018-21), 111 Project (B17021), the Graduate Students Innovation Project of Jiangsu Province in China (no. KYCX17_1435 to S.Y.C.) and the Excellent Doctoral Cultivation Project of Jiangnan University. The authors thanks L. Rohrbach for the technical support in the surface tension measurements.

6.5 Experimental Data

6.5.1 Materials and Methods

For the general materials and methods, please refer to section A, Materials and Methods, in the Appendix.

Nile Red Fluorescence Assay. The self-assembly of the **MA** was assessed by incorporation of the hydrophobic solvatochromic probe Nile Red (9-diethylamino-5-benzo[α]phenoxazinone), which exhibits a blue shift emission upon inclusion in hydrophobic environments.[32,69] Nile Red dissolved at 1 mM in ethanol was diluted to a solution, with a final concentration of 250 nM. As a result, all samples contain 0.25% ethanol, which is expected to not interfere with the self-assembly behavior. Using a JASCO FP6200 fluorometer, the buffer solutions of **MA** (concentration: 2.0 x 10^{-5} to 2.0 mM) and Nile Red (250 nM) were excited at 550 nm and the spectra were recorded over a wavelength range of 580 – 750 nm. Blue shifts were calculated by subtracting the emission wavelength of Nile Red in buffer solution (Tris-EDTA, pH 7.4) from the emission wavelength of the sample. Blue shifts were plotted against concentrations to determine a critical aggregation concentration.

Cryogenic Transmission Electron Microscopy. For analysis by cryo-transmission electron microscopy (cryo-TEM), the **MA** buffer solutions (2.5 μL, 2.0 mM) were placed on a glow-discharged holy carbon coated grid (Quantifoil 3.5/1, QUANTIFOIL Micro Tools GmbH, Großlöbichau, Germany). After blotting, the grid was rapidly frozen in liquid ethane (Vitrobot, FEI, Eindhoven, The Netherlands) and stored in liquid nitrogen until measured. Grids were observed in a Gatan model 626 cryo-stage in a Tecnai T20 (FEI, Eindhoven, The Netherlands) cryo-electron microscope operating at 120 or 200 keV. Images were recorded under low-dose conditions on a slow-scan CCD camera.

Surface Tension Measurements. The surface tension was measured by a drop-shape analysis system (Optical contact angle measuring and contour analysis systems, Data Physics, Germany), which is based on the fitting of the pendant drop shape of the measured solutions with the Young−Laplace equation of capillarity.[74–76]

The drop volume of the freshly prepared solution was precisely controlled at 2 μL. As shown in Figure 6.13, a humidifier and a cover were used to maintain the relative humidity at ~65%, minimizing the water evaporation. The humidity and temperature were monitored by a Humidity/Temperature Monitor (800016, SPER SCIENTIFIC, United States). All the measurements were performed in triplicate.

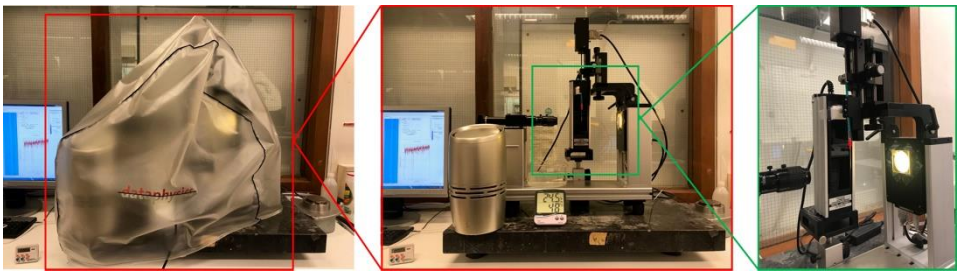

Figure 6.13 *Photographs of surface tension measurement instrument.*

6.5.2 Synthesis and Characterization

Stable *trans*-2:

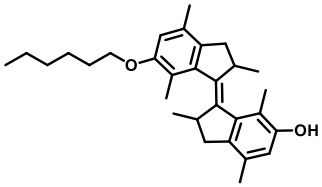

To a MeCN suspension (14 mL) of stable *trans*-**1** (200 mg, 0.57 mmol), K_2CO_3 (238 mg, 1.72 mmol) and tetra-*n*-butylammonium iodide (636 mg, 1.72 mmol), 1-bromohexane (80.52 mg, 0.49 mmol) was added at room temperature, whereupon the mixture was stirred at 75 °C for 16 h. After cooling to room temperature, the reaction mixture was acidified using a saturated aqueous NH_4Cl solution to pH = 6~7, followed by washing with water (30 mL) and ethyl acetate (30 mL). The combined organic layers were washed with brine and dried over Na_2SO_4. The solvent was removed by rotary evaporation and the residue was purified by column chromatography on SiO_2 (ethyl acetate/pentane; v/v = 1/19, R_f = 0.4) to yield stable *trans*-**2** (91 mg, 0.21 mmol, 43% yield) as a white solid. The corresponding compound of stable *trans*-**2** was immediately subjected to the next synthesis step due to degradation problems during storage.

Stable *cis*-2:

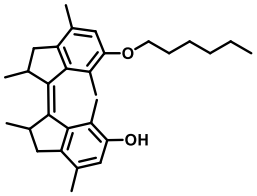

Using a procedure similar to that for stable *trans*-**2**, stable *cis*-**2** was purified by column chromatography on SiO_2 (ethyl acetate/pentane; v/v = 1/19, R_f = 0.6) and obtained as a white solid (112 mg, 0.26 mmol, 53% yield) from stable *cis*-**1** and 1-bromohexane. The corresponding compound of stable *cis*-**2** was immediately subjected to the next synthesis step due to degradation problems during storage.

Stable *trans*-4:

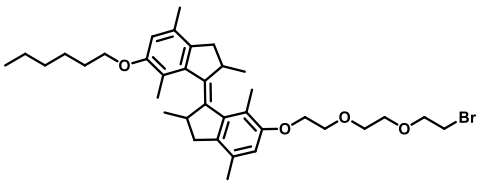

A mixture of stable *trans*-**2** (200 mg, 0.46 mmol), **3** (255 mg, 0.92 mmol) and cesium carbonate (450 mg, 1.38 mmol) in DMF/MeCN (4 mL/14 mL) was heated at 80 °C for 16 h. The reaction mixture was allowed to cool to room temperature and then washed with water (50 mL) and ethyl acetate (30 mL). The combined organic layers were washed with brine and dried over Na_2SO_4. The solvent was removed by rotary evaporation. The residue was purified by column chromatography on SiO_2 (ethyl acetate/pentane; v/v =2/23, R_f = 0.56) to yield stable *trans*-**4** (125 mg, 0.20 mmol, 43% yield) as a colorless oil.

^{1}H NMR (400 MHz, $CDCl_3$) δ (ppm) 6.55 (d, J = 3.3 Hz, 2H), 4.31 – 3.60 (m, 12H), 3.49 (t, J = 6.3 Hz, 2H), 2.96 – 2.83 (m, 2H), 2.60 (dd, J = 14.2, 5.5 Hz, 2H), 2.31 (d, J = 3.6 Hz, 6H), 2.21 – 2.11 (m, 8H), 1.89 – 1.78 (m, 2H), 1.59 – 1.47 (m, 2H), 1.42 – 1.34 (m, 4H), 1.09 (dd, J = 6.5, 2.8 Hz, 6H), 0.93 (t, J = 6.8 Hz, 3H).

^{13}C NMR (100 MHz, $CDCl_3$) δ (ppm) 156.5, 156.2, 142.7, 142.5, 142.0, 141.7, 134.5, 134.0, 131.4, 131.3, 120.8, 120.7, 111.4, 111.0, 71.4, 71.4, 71.2, 71.1, 70.8, 70.7, 70.4, 88.6, 88.4, 42.3, 42.3, 38.5, 31.8, 30.5, 29.8, 26.0, 22.8, 19.3, 18.8, 16.4, 16.4, 14.2.

HRMS (ESI) calculated for $C_{36}H_{52}BrO_4$ [M+H] is 627.3044, found 627.3038.

Stable *cis*-4:

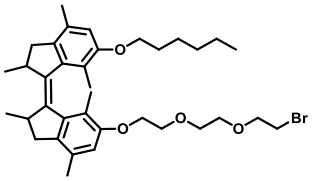

Using a procedure similar to that for stable *trans*-**4**, stable *cis*-**4** was purified by column chromatography on SiO_2 (ethyl acetate/pentane; v/v =1/24, R_f = 0.5) and obtained as a pale yellow oil (144 mg, 0.23 mmol, 50% yield) from stable *cis*-**2** and **3**.

^{1}H NMR (400 MHz, $CDCl_3$) δ (ppm) 6.54 (d, J = 5.5 Hz, 2H), 4.20 – 3.64 (m, 12H), 3.44 (t, J = 6.3 Hz, 2H), 3.36 – 3.33 (m, 2H), 3.04 (dd, J = 14.5, 6.2 Hz, 2H), 2.38 (d, J = 14.5 Hz, 2H), 2.25 (s, 6H), 1.81 – 1.69 (m, 2H), 1.50 – 1.29 (m, 12H), 1.07 (dd, J = 6.8, 2.3 Hz, 6H), 0.89 (t, J = 7.0 Hz, 3H).

^{13}C NMR (100 MHz, $CDCl_3$) δ (ppm) 156.0, 155.7,142.4, 142.1, 141.2, 141.0, 136.6, 136.0, 130.6, 130.4, 122.7, 122.5, 112.3, 111.7, 71.4, 71.4, 71.1, 71.0, 70.7, 70.6, 70.2, 70.2, 68.8, 68.7, 68.6, 42.0, 42.0, 38.2, 31.7, 31.7, 30.4, 29.7, 26.0, 22.7, 20.6, 20.6, 19.0, 19.0, 14.4, 14.4, 14.2.

HRMS (ESI) calculated for $C_{36}H_{52}BrO_4$ [M+H] is 627.3044, found 627.3038.

Stable *trans*-MA:

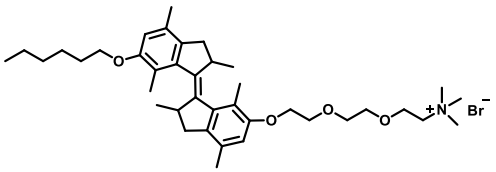

A mixture of stable *trans*-**4** (100 mg, 0.16 mmol) and a 4.3 M NMe_3 solution in ethanol (4 mL) was stirred in a pressure tube at 50 ºC for 24 h. After cooling to room temperature, the solvent was removed in vacuum and the residue was washed with diethyl ether (2 mL) and pentane (20 mL). The precipitate was filtered off to obtain stable *trans*-**MA** (96 mg, 0.14 mmol, 90% yield) as a white solid.

^{1}H NMR (400 MHz, $CDCl_3$) δ (ppm) 6.52 (d, J = 3.3 Hz, 2H), 4.16 – 3.83 (m, 10H), 3.71 – 3.75 (m, 4H), 3.47 (s, 9H), 2.94 – 2.79 (m, 2H), 2.57 (dd, J = 14.1, 5.4 Hz, 2H), 2.27 (d, J = 5.3 Hz, 6H), 2.15 – 2.11 (m, 8H), 1.84 – 1.77 (m, 2H), 1.51 – 1.49 (m, 2H), 1.35 – 1.34 (m, 4H), 1.06 (dd, J = 6.3, 3.0 Hz, 6H), 0.90 (t, J = 6.9 Hz, 3H).

^{13}C NMR (100 MHz, $CDCl_3$) δ (ppm) 157.3, 156.8, 143.5, 143.1, 142.8, 142.3, 135.5, 134.6, 132.4, 132.1, 121.4, 121.2, 112.2, 111.9, 71.5, 71.4, 71.0, 69.3, 69.2, 66.5,

66.5, 66.5, 66.2, 55.6, 43.1, 43.0, 39.2, 39.2, 32.5, 30.5, 26.8, 23.5, 20.1, 20.1, 19.6, 19.6, 17.2, 17.1, 15.0.

HRMS (ESI) calculated for $C_{39}H_{60}NO_4$ is 606.4517, found 606.4513.

Stable *cis*-MA:

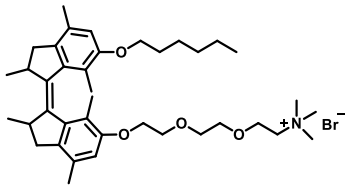

Using a procedure similar to that for stable *trans*-**MA**, stable *cis*-**MA** was obtained as a pale yellow solid (96 mg, 0.14 mmol, 90% yield) from stable *cis*-**4** and NMe_3 solution.

^{1}H NMR (400 MHz, $CDCl_3$) δ (ppm) 6.50 (d, J = 4.3 Hz, 2H), 4.08 – 4.05 (m, 1H), 3.98 – 3.88 (m, 6H), 3.81 – 3.73 (m, 3H), 3.66 – 3.59 (m, 4H), 3.36 – 3.25 (m, 11H), 3.00 (dd, J = 14.6, 6.0 Hz, 2H), 2.34 (d, J = 14.5 Hz, 2H), 2.21 (s, 6H), 1.69 (m, 2H), 1.45 – 1.22 (m, 12H), 1.02 (dd, J = 6.5, 2.5 Hz, 6H), 0.84 (t, J = 6.8 Hz, 3H).

^{13}C NMR (100 MHz, $CDCl_3$) δ (ppm) 156.6, 156.3, 143.2, 142.9, 142.1, 141.6, 137.6, 137.0, 131.6, 131.4, 123.2, 123.1, 113.2, 112.8, 71.4, 71.3, 70.9, 69.8, 69.6, 66.4, 66.4, 66.4, 66.1, 55.5, 42.7, 42.7, 38.9, 32.4, 30.4, 26.6, 23.4, 23.2, 21.3, 21.3, 19.7, 19.7, 15.2, 15.1, 14.9.

HRMS (ESI) calculated for $C_{39}H_{60}NO_4$ is 606.4517, found 606.4517.

6.6 References

(1) Fletcher, D. A.; Mullins, R. D. Cell Mechanics and the Cytoskeleton. *Nature* **2010**, *463* (7280), 485–492.
(2) Huber, F.; Schnauß, J.; Rönicke, S.; Rauch, P.; Müller, K.; Fütterer, C.; Käs, J. Emergent Complexity of the Cytoskeleton: From Single Filaments to Tissue. *Adv. Phys.* **2013**, *62* (1), 1–112.
(3) Lino, T. Assembly of Salmonella Flagellin in Vitro and in Vivo. *J. Supramol. Struct.* **1974**, *2*, 372–384.
(4) Simmons, N. S.; Blout, E. R. The Structure of Tobacco Mosaic Virus and its Components: Ultraviolet Optical Rotatory Dispersion. *Biophys. J.* **1960**, *1* (1), 55–62.
(5) Chapman, D. Phase Transitions and Fluidity Characteristics of Lipids and Cell Membranes. *Q. Rev. Biophys.* **1975**, *8*, 185–235.
(6) Cooper, R. A. Influence of Increased Membrane Cholesterol on Membrane Fluidity and Cell Function in Human Red Blood Cells. *J. Supramol. Struct.* **1978**, *8*, 413–430.
(7) Lehn, J. M. Supramolecular Polymer Chemistry-Scope and Perspective. *Polym. Int.* **2002**, *51* (10), 825–839.

(8) Oshovsky, G. V.; Reinhoudt, D. N.; Verboom, W. Supramolecular Chemistry in Water. *Angew. Chem. Int. Ed.* **2007**, *46* (14), 2366–2393.
(9) de Greef, T. F. A.; Meijer, E. W. Supramolecular Polymers. *Nature* **2008**, *453*, 171–173.
(10) Palmer, L. C.; Stupp, S. I. Molecular Self-Assembly into One-Dimensional Nanostructures. *Acc. Chem. Res.* **2008**, *41*, 1674–1684.
(11) Wojtecki, R. J.; Meador, M. A.; Rowan, S. J. Using the Dynamic Bond to Access Macroscopically Responsive Structurally Dynamic Polymers. *Nat. Mater.* **2011**, *10*, 14–27.
(12) Krieg, E.; Rybtchinski, B. Noncovalent Water-Based Materials: Robust yet Adaptive. *Chem. Eur. J.* **2011**, *17*, 9016–9026.
(13) Yan, X.; Wang, F.; Zheng, B.; Huang, F. Stimuli-Responsive Supramolecular Polymeric Materials. *Chem. Soc. Rev.* **2012**, *41*, 6042–6065.
(14) Li, S. L.; Xiao, T.; Lin, C.; Wang, L. Advanced Supramolecular Polymers Constructed by Orthogonal Self-Assembly. *Chem. Soc. Rev.* **2012**, *41*, 5950–5968.
(15) Aida, T.; Meijer, E. W.; Stupp, S. I. Functional Supramolecular Polymers. *Science* **2012**, *335*, 813–817.
(16) Dong, R.; Zhou, Y.; Huang, X.; Zhu, X.; Lu, Y.; Shen, J. Functional Supramolecular Polymers for Biomedical Applications. *Adv. Mater.* **2015**, *27*, 498–526.
(17) Smith, K. H.; Tejeda-Montes, E.; Poch, M.; Mata, A. Integrating Top-down and Self-Assembly in the Fabrication of Peptide and Protein-Based Biomedical Materials. *Chem. Soc. Rev.* **2011**, *40*, 4563–4577.
(18) Mulder, A.; Huskens, J.; Reinhoudt, D. N. Multivalency in Supramolecular Chemistry and Nanofabrication. *Org. Biomol. Chem.* **2004**, *2*, 3409–3424.
(19) Hamley, I. W. Self-Assembly of Amphiphilic Peptides. *Soft Matter* **2011**, *7*, 4122–4138.
(20) Iamsaard, S.; Aßhoff, S. J.; Matt, B.; Kudernac, T.; Cornelissen, J. J. L. M.; Fletcher, S. P.; Katsonis, N. Conversion of Light into Macroscopic Helical Motion. *Nat. Chem.* **2014**, *6*, 229–235.
(21) Harada, A.; Takashima, Y.; Nakahata, M. Supramolecular Polymeric Materials via Cyclodextrin Guest Interactions. *Acc. Chem. Res.* **2014**, *47*, 2128–2140.
(22) van Oosten, C. L.; Bastiaansen, C. W. M.; Broer, D. J. Printed Artificial Cilia from Liquid-Crystal Network Actuators Modularly Driven by Light. *Nat. Mater.* **2009**, *8*, 677–682.
(23) White, T. J.; Broer, D. J. Programmable and Adaptive Mechanics with Liquid Crystal Polymer Networks and Elastomers. *Nat. Mater.* **2015**, *14*, 1087–1098.
(24) Li, Q.; Fuks, G.; Moulin, E.; Maaloum, M.; Rawiso, M.; Kulic, I.; Foy, J. T.; Giuseppone, N. Macroscopic Contraction of a Gel Induced by the Integrated Motion of Light-Driven Molecular Motors. *Nat. Nanotechnol.* **2015**, *10*, 161–165.
(25) Iwaso, K.; Takashima, Y.; Harada, A. Fast Response Dry-Type Artificial Molecular Muscles with [C_2] Daisy Chains. *Nat. Chem.* **2016**, *8*, 625–632.
(26) Foy, J. T.; Li, Q.; Goujon, A.; Colard-Itté, J. R.; Fuks, G.; Moulin, E.; Schiffmann, O.; Dattler, D.; Funeriu, D. P.; Giuseppone, N. Dual-Light Control of Nanomachines That Integrate Motor and Modulator Subunits. *Nat. Nanotechnol.* **2017**, *12*, 540–545.
(27) Gelebart, A. H.; Mulder, D. J.; Varga, M.; Konya, A.; Vantomme, G. Making Waves in a Photoactive Polymer Film. *Nature* **2017**, *546*, 632–636.
(28) Aßhoff, S. J.; Lancia, F.; Iamsaard, S.; Matt, B.; Kudernac, T.; Fletcher, S. P.; Katsonis, N. High-Power Actuation from Molecular Photoswitches in Enantiomerically Paired Soft Springs. *Angew. Chem. Int. Ed.* **2017**, *56*, 3261–3265.
(29) Camacho-Lopez, M.; Finkelmann, H.; Palffy-Muhoray, P.; Shelley, M. Fast Liquid-Crystal Elastomer Swims into the Dark. *Nat. Mater.* **2004**, *3*, 307–310.

(30) Ikeda, T.; Mamiya, J.; Yu, Y. Artificial Muscles Photomechanics of Liquid-Crystalline Elastomers and Other Polymers. *Angew. Chem. Int. Ed.* **2007**, *46*, 506–528.

(31) Chen, J.; Leung, F. K. C.; Stuart, M. C. A.; Kajitani, T.; Fukushima, T.; van der Giessen, E.; Feringa, B. L. Artificial Muscle-like Function from Hierarchical Supramolecular Assembly of Photoresponsive Molecular Motors. *Nat. Chem.* **2018**, *10* (2), 132–138.

(32) Leung, F. K. C.; van den Enk, T.; Kajitani, T.; Chen, J.; Stuart, M. C. A.; Kuipers, J.; Fukushima, T.; Feringa, B. L. Supramolecular Packing and Macroscopic Alignment Controls Actuation Speed in Macroscopic Strings of Molecular Motor Amphiphiles. *J. Am. Chem. Soc.* **2018**, *140* (50), 17724–17733.

(33) Leung, F. K. C.; Stuart, M. C. A.; Kajitani, T.; Fukushima, T.; Feringa, B. L. Dual-Controlled Macroscopic Motions in a Supramolecular Hierarchical Assembly of Motor Amphiphiles. *Angew. Chem. Int. Ed.* **2019**, *58* (32), 10985-10989.

(34) Ikegami, T.; Kageyama, Y.; Obara, K.; Takeda, S. Dissipative and Autonomous Square-Wave Self-Oscillation of a Macroscopic Hybrid Self-Assembly under Continuous Light Irradiation. *Angew. Chem. Int. Ed.* **2016**, *55*, 8239–8243.

(35) Irie, M.; Fukaminato, T.; Matsuda, K.; Kobatake, S. Photochromism of Diarylethene Molecules and Crystals : Memories , Switches , and Actuators. *Chem. Rev.* **2014**, *114*, 12174–12277.

(36) Kitagawa, D.; Nishi, H.; Kobatake, S. Photoinduced Twisting of a Photochromic Diarylethene Crystal. *Angew. Chem. Int. Ed.* **2013**, *52*, 9320–9322.

(37) Morimoto, M.; Irie, M. A Diarylethene Cocrystal that Converts Light into Mechanical Work. *J. Am. Chem. Soc.* **2010**, *132*, 14172–14178.

(38) Goujon, A.; Mariani, G.; Lang, T.; Moulin, E.; Rawiso, M.; Buhler, E.; Giuseppone, N. Controlled Sol−Gel Transitions by Actuating Molecular Machine Based Supramolecular Polymers. *J. Am. Chem. Soc.* **2017**, *139*, 4923–4928.

(39) Wu, A.; Sun, P.; Sun, N.; Zheng, L. Responsive Self-Assembly of Supramolecular Hydrogel Based on Zwitterionic Liquid Asymmetric Gemini Guest. *Chem. Eur. J.* **2018**, *24*, 10452–10459.

(40) Choi, Y. J.; Kim, J. T.; Yoon, W. J.; Kang, D. G.; Park, M.; Kim, D. Y.; Lee, M. hoon; Ahn, S. kyun; Jeong, K. Azobenzene Molecular Machine: Light-Induced Wringing Gel Fabricated from Asymmetric Macrogelator. *ACS Macro Lett.* **2018**, *7*, 576–581.

(41) Wang, C.; Chen, Q.; Sun, F.; Zhang, D.; Zhang, G.; Huang, Y.; Zhao, R.; Zhu, D. Multistimuli Responsive Organogels Based on a New Gelator Featuring Tetrathiafulvalene and Azobenzene Groups : Reversible Tuning of the Gel-Sol Transition by Redox Reactions and Light Irradiation. *J. Am. Chem. Soc.* **2010**, *132*, 3092–3096.

(42) Koumura, N.; Kudo, M.; Tamaoki, N. Photocontrolled Gel-to-Sol-to-Gel Phase Transitioning of Meta-Substituted Azobenzene Bisurethanes through the Breaking and Reforming of Hydrogen Bonds. *Langmuir* **2004**, *20*, 9897–9900.

(43) Zhou, Y.; Xu, M.; Yi, T.; Xiao, S.; Zhou, Z.; Li, F.; Huang, C. Morphology-Tunable and Photoresponsive Properties in a Self-Assembled Two-Component Gel System. *Langmuir* **2007**, *23*, 202–208.

(44) Kim, J. H.; Seo, M.; Kim, Y. J.; Kim, S. Y. Rapid and Reversible Gel-Sol Transition of Self-Assembled Gels Induced by Photoisomerization of Dendritic Azobenzenes. *Langmuir* **2009**, *25*, 1761–1766.

(45) van Herpt, J. T.; Areephong, J.; Stuart, M. C. A.; Browne, W. R.; Feringa, B. L. Light-Controlled Formation of Vesicles and Supramolecular Organogels by a

Cholesterol-Bearing Amphiphilic Molecular Switch. *Chem. Eur. J.* **2014**, *20* (6), 1737–1742.

(46) Denkov, N. D.; Tcholakova, S.; Golemanov, K.; Ananthpadmanabhan, K. P.; Lips, A. The Role of Surfactant Type and Bubble Surface Mobility in Foam Rheology. *Soft Matter* **2009**, *5*, 3389–3408.

(47) Mileva, E.; Exerowa, D. Amphiphilic Nanostructures in Foam Films. *Curr. Opin. Colloid Interface Sci.* **2008**, *13*, 120–127.

(48) Fameau, A. L; Salonen, A. Effect of Particles and Aggregated Structures on the Foam Stability and Aging. *Comptes Rendus Phys.* **2014**, *15*, 748–760.

(49) Fameau, A. L.; Lam, S.; Velev, O. D. Multi-Stimuli Responsive Foams Combining Particles and Self-Assembling Fatty Acids. *Chem. Sci.* **2013**, *4*, 3874–3881.

(50) Wan, Z.; Sun, Y.; Zhou, F.; Guo, J.; Hu, S.; Yang, X. Long-Lived and Thermoresponsive Emulsion Foams Stabilized by Self-Assembled Saponin Nano Fi Brils and Fibrillar Network. *Langmuir* **2018**, *34*, 3971–3980.

(51) Chen, S.; Zhang, Y.; Chen, K.; Yin, Y.; Wang, C. Insight into a Fast-Phototuning Azobenzene Switch for Sustainably Tailoring the Foam Stability. *ACS Appl. Mater. Interfaces* **2017**, *9* (15), 13778–13784.

(52) Chen, S.; Wang, C.; Yin, Y.; Chen, K. Synthesis of Photo-Responsive Azobenzene Molecules with Different Hydrophobic Chain Length for Controlling Foam Stability. *RSC Adv.* **2016**, *6* (65), 60138–60144.

(53) Chevallier, E.; Monteux, C.; Lequeux, F.; Tribet, C. Photofoams: Remote Control of Foam Destabilization by Exposure to Light Using an Azobenzene Surfactant. *Langmuir* **2012**, *28* (5), 2308–2312.

(54) Chevallier, E.; Saint-Jalmes, A.; Cantat, I.; Lequeux, F.; Monteux, C. Light Induced Flows Opposing Drainage in Foams and Thin-Films Using Photosurfactants. *Soft Matter* **2013**, *9* (29), 7054–7060.

(55) Mamane, A.; Chevallier, E.; Olanier, L.; Lequeux, F.; Monteux, C. Optical Control of Surface Forces and Instabilities in Foam Films Using Photosurfactants. *Soft Matter* **2017**, *13* (6), 1299–1305.

(56) Lei, L.; Xie, D.; Song, B.; Jiang, J.; Pei, X.; Cui, Z. Photoresponsive Foams Generated by a Rigid Surfactant Derived from Dehydroabietic Acid. *Langmuir* **2017**, *33* (32), 7908–7916.

(57) Shang, T.; Smith, K. A.; Hatton, T. A. Photoresponsive Surfactants Exhibiting Unusually Large, Reversible Surface Tension Changes under Varying Illumination Conditions. *Langmuir* **2003**, *19* (26), 10764–10773.

(58) Jiang, J.; Ma, Y.; Cui, Z. Smart Foams Based on Dual Stimuli-Responsive Surfactant. *Colloids Surfaces A* **2017**, *513*, 287–291.

(59) Shi, S.; Yin, T.; Shen, W. Switchable Foam Control by a New Surface-Active Ionic Liquid. *RSC Adv.* **2016**, *6* (96), 93621–93625.

(60) Chen, S.; Zhang, W.; Wang, C.; Sun, S. A Recycled Foam Coloring Approach Based on the Reversible Photo-Isomerization of an Azobenzene Cationic Surfactant. *Green Chem.* **2016**, *18* (14), 3972–3980.

(61) Coleman, A. C.; Beierle, J. M.; Stuart, M. C. A.; Maciá, B.; Caroli, G.; Mika, J. T.; van Dijken, D. J.; Chen, J.; Browne, W. R.; Feringa, B. L. Light-Induced Disassembly of Self-Assembled Vesicle-Capped Nanotubes Observed in Real Time. *Nat. Nanotechnol.* **2011**, *6* (9), 547–552.

(62) Erne, P. M.; van Bezouwen, L. S.; Štacko, P.; van Dijken, D. J.; Chen, J.; Stuart, M. C. A.; Boekema, E. J.; Feringa, B. L. Loading of Vesicles into Soft Amphiphilic Nanotubes Using Osmosis. *Angew. Chem. Int. Ed.* **2015**, *54* (50), 15122–15127.

(63) van Dijken, D. J.; Chen, J.; Stuart, M. C. A.; Hou, L.; Feringa, B. L. Amphiphilic Molecular Motors for Responsive Aggregation in Water. *J. Am. Chem. Soc.* **2016**, *138* (2), 660–669.
(64) Song, S.; Song, A.; Hao, J. Self-Assembled Structures of Amphiphiles Regulated via Implanting External Stimuli. *RSC Adv.* **2014**, *4* (79), 41864–41875.
(65) Neubauer, T. M.; van Leeuwen, T.; Zhao, D.; Lubbe, A. S.; Kistemaker, J. C. M.; Feringa, B. L. Asymmetric Synthesis of First Generation Molecular Motors. *Org. Lett.* **2014**, *16*, 4220–4223.
(66) Li, Y.; Dong, J.; Xun, Z.; Zeng, Y.; Yu, T.; Han, Y.; Chen, J.; Li, Y. Y.; Yang, G. A Versatile and Robust Vesicle Based on a Photocleavable Surfactant for Two-Photon-Tuned Release. *Chem. Eur. J.* **2013**, *19* (24), 7931–7936.
(67) Wang, J.; Feringa, B. L. Dynamic Control of Chiral Space in a Catalytic Asymmetric Reaction Using a Molecular Motor. *Science* **2011**, *331*, 1429–1432.
(68) Lubbe, A. S.; Böhmer, C.; Tosi, F.; Szymanski, W.; Feringa, B. L. Molecular Motors in Aqueous Environment. *J. Org. Chem.* **2018**, *83* (18), 11008–11018.
(69) Tantakitti, F.; Boekhoven, J.; Wang, X.; Kazantsev, R. V.; Yu, T.; Li, J.; Zhuang, E.; Zandi, R.; Ortony, J. H.; Newcomb, C. J.; Palmer, L. C.; Shekhawat, G. S.; Olvera de la Cruz, M.; Schatz, G. C.; Stupp, S. I. Energy Landscapes and Functions of Supramolecular Systems. *Nat. Mater.* **2016**, 15 (4), 469–476.
(70) Yu, H.; Wang, Y.; Zhong, Y.; Mao, Z.; Tan, S. Foam Properties and Application in Dyeing Cotton Fabrics with Reactive Dyes. *Color. Technol.* **2014**, *130* (4), 266–272.
(71) Fameau, A. L.; Houinsou-Houssou, B.; Ventureira, J. L.; Navailles, L.; Nallet, F.; Novales, B.; Douliez, J. Self-Assembly , Foaming , and Emulsifying Properties of Sodium Alkyl Carboxylate / Guanidine Hydrochloride Aqueous Mixtures. *Langmuir* **2011**, *27*, 4505–4513.
(72) Fameau, A. L.; Saint-Jalmes, A.; Cousin, F.; Houssou, B. H.; Novales, B.; Navailles, L.; Nallet, F.; Gaillard, C.; Boue, F.; Douliez, J.-P. Smart Foams : Switching Reversibly between Ultrastable and Unstable Foams. *Angew. Chem. Int. Ed.* **2011**, *50*, 8264–8269.
(73) Fameau, A. L.; Cousin, F.; Derrien, R.; Saint-Jalmes, A. Design of Responsive Foams with an Adjustable Temperature Threshold of Destabilization. *Soft Matter* **2018**, *14*, 2578–2581.
(74) Shin, J. Y.; Abbott, N. L. Using Light to Control Dynamic Surface Tensions of Aqueous Solutions of Water Soluble Surfactants. *Langmuir* **1999**, *15* (13), 4404–4410.
(75) Cicciarelli, B. A.; Hatton, T. A.; Smith, K. A. Dynamic Surface Tension Behavior in a Photoresponsive Surfactant System. *Langmuir* **2007**, *23* (9), 4753–4764.
(76) Cicciarelli, B. A.; Elia, J. A.; Hatton, T. A.; Smith, K. A. Temperature Dependence of Aggregation and Dynamic Surface Tension in a Photoresponsive Surfactant System. *Langmuir* **2007**, *23* (16), 8323–8330.